EJN
European Journal of Neuroscience

European Journal of Neuroscience, Vol. 28, pp. 447–459, 2008 doi:10.1111/j.1460-9568.2008.06358.x

Comparison of spatial integration and surround suppression characteristics in spiking activity and the local field potential in macaque V1

M. A. Gieselmann and A. Thiele
Institute of Neuroscience, Henry Wellcome Building, Framlington Place Newcastle University, Newcastle upon Tyne, NE2 4HH, UK

Keywords: contextual influences, gamma oscillations, primary visual cortex

Abstract

Neurons in primary visual cortex exhibit well documented centre–surround receptive field organization, whereby the centre is dominated by excitatory influences and the surround is generally dominated by inhibitory influences. These effects have largely been established by measuring the output of neurons, i.e. their spiking activity. How excitation and inhibition are reflected in the local field potential (LFP) is little understood. As this can bear on the interpretation of human fMRI BOLD data and on our understanding of the mechanisms of local field potential oscillations, we measured spatial integration and centre–surround properties in single- and multiunit recordings of V1 in the awake fixating macaque monkey, and compared these to spectral power in different frequency bands of simultaneously recorded LFPs. We quantified centre–surround organization by determining the size of the summation and suppression area in spiking activity as well as in different frequency bands of the LFP, with the main focus on the gamma band. Gratings extending beyond the summation area usually inhibited spiking activity while the LFP gamma-band activity increased monotonically for all grating sizes. This increase was maximal for stimuli infringing upon the near classical receptive field surround, where suppression started to dominate spiking activity. Thus, suppressive influences in primary cortex can be inferred from spiking activity, but they also seem to affect specific features of gamma-band LFP activity.

Introduction

Extracellular neuronal recordings typically convey two types of signals: (i) spike signals, containing action potentials of neurons in the vicinity of the electrode tip; and (ii) the local field potential (LFP), containing low-frequency fluctuations in the electrical potential generated by local and more remote neurons. While the physiological basis of the spike signal is well defined, some debate continues regarding the underlying mechanisms of the LFP. However, it is accepted that the LFP mainly represents dendritic activity from an area within ~500 μm around the electrode tip (Kruse & Eckhorn, 1996), reflecting the intracortical processing as well as inputs from other brain areas (Mitzdorf, 1987; Logothetis, 2002; Buzsaki, 2004). The LFP therefore carries the summed information of dendritic activity from excitatory cells and inhibitory interneurons. The functional significance of the LFP has been demonstrated in contexts such as motor intentions (Scherberger *et al.*, 2005), working memory (Pesaran *et al.*, 2002), visual attention (Womelsdorf *et al.*, 2006), binocular rivalry (Gail *et al.*, 2004) and visual object representation (Kreiman *et al.*, 2006). Notably, the LFP signal can carry information that differs substantially from the spike signal. Wilke *et al.* (2006) showed that in early visual areas lower frequency fluctuations of the LFP are better correlated with perception than the spike signal. Additional interest in the LFP has been fuelled by functional magnetic resonance imaging (fMRI) studies. FMRI studies generally use the blood oxygen level-dependent (BOLD) signal to infer brain function, and the LFP appears to be a better predictor of BOLD responses than spiking activity (Logothetis *et al.*, 2001; Kayser *et al.*, 2004; Niessing *et al.*, 2005; Nir *et al.*, 2007). Thus, understanding tuning properties of the LFP signal and understanding the neuronal computations it reflects can have important implications for the interpretation of the BOLD signal. We were particularly interested to what extent the LFP reflects excitatory and inhibitory influences which are seen in spiking activity when analyzing centre–surround mechanisms (Hubel & Wiesel, 1968; Nelson & Frost, 1978; Hammond & MacKay, 1981; Allman *et al.*, 1985; DeAngelis *et al.*, 1994; Li & Li, 1994; Bauer *et al.*, 1995; Raiguel *et al.*, 1995; Jones *et al.*, 2001).

As the contribution of excitatory and inhibitory influences in centre–surround mechanisms can be quantified by measuring spatial integration properties in V1 (Sceniak *et al.*, 1999, 2001; Kapadia *et al.*, 2000; Roberts *et al.*, 2005, 2007; Ichida *et al.*, 2007), we measured spatial summation properties of multiunit (MU) spiking activity and compared it to the simultaneously recorded LFP, focusing mostly on the gamma frequency range. We show that the characteristics of spatial summation found in the power spectrum of the LFP is complementary to the one found in the MU activity. In accord with previous studies, signatures of suppression were found in MU spiking activity when stimuli extended beyond the classical receptive field, and these were probably mediated by inhibitory interneurons. Conversely, the gamma-band LFP signal never showed features of suppression and thus did not directly reveal contributions from inhibitory neurons. However, certain features of spectral power in the gamma-band LFP reflected processes that are usually assigned to GABAa inhibitory processes and which were deducible from our simultaneously recorded spiking activity. We discuss these findings in relation to proposed neuronal network mechanisms of gamma oscillation induction (Traub *et al.*, 1996b; Wang & Buzsaki, 1996;

Correspondence: Dr A. Thiele, as above.
E-mail: alex.thiele@ncl.ac.uk

Received 14 March 2008, revised 21 May 2008, accepted 9 June 2008

Brunel & Wang, 2003; Tiesinga & Sejnowski, 2004) and possible implications for interpreting fMRI studies examining spatial summation in the BOLD signal (Williams *et al.*, 2003; Zenger-Landolt & Heeger, 2003; Delicato *et al.*, 2006).

Materials and methods

Animals

We recorded extracellular neuronal activity from three hemispheres in two male macaque monkeys (*Macacca mulatta*). Animals were implanted with a custom-made head-holding device and recording chambers made of Tecapeek GF for compatibility in fMRI settings. A scleral search coil was implanted for monitoring eye position. Surgical procedures were performed under aseptic conditions and general anesthesia (1–3% sevoflurane) as described in detail previously (Thiele *et al.*, 2006). Experiments and surgeries were performed in accordance with the European Communities Council Directive 1986 (86/609/EEC), the National Institutes of Health (Guidelines for Care and Use of Animals for Experimental Procedures), the Society for Neurosciences Policies on the Use of Animals and Humans in Neuroscience Research, and the UK Animals Scientific Procedures Act.

Data acquisition

Experimental timing, behavioral control and stimulus presentation was controlled by Cortex (DOS-Version 5.95; NIMH, http://www.cortex.salk.edu) running on IBM-compatible personal computers. Neuronal activity was recorded with glass-coated tungsten electrodes (1.0–3.0 MΩ). Reference electrodes were 150-μm-thick tungsten wires attached to the electrode (ending ∼10–15 mm above the electrode tip). Electrodes were advanced by a hydraulic microdrive (Narishige, Tokyo, Japan). The recorded electrical signal was split into two channels. The signal of one channel was bandpass-filtered between 0.6 and 9 kHz to extract spiking activity (Neuralynx, Inc., Bozeman, Montana). The waveforms of all spikes that exceeded a threshold set by the experimenter were sampled at 32 kHz. Offline sorting of these MU spike samples was carried out based on waveform features (Neuralynx spike sorting software, Version 2.10). The second channel was bandpass-filtered between 1 and 475 Hz and digitized at a rate of 1.01 or 1.83 kHz to obtain the LFP signal.

Visual stimuli and protocol

Monkeys were trained to hold their gaze within ± 0.5° of a fixation spot (0.03–0.08° diameter) while visual stimuli were presented on a video CRT monitor (1600 × 1200 at 85 Hz or 1280 × 1024 at 110 Hz). Stimuli were presented on a gray background at a mean luminance of 89 or 56 cd/m^2 (these correspond to the mean luminance of two different monitors at an RGB gray level setting of 128; the mean luminance difference between these two settings had no effect on the data).

For each recording site we initially determined the location of the receptive field (RF) as well as the optimal orientation, spatial frequency and phase of a stationary sinusoidal grating. The location of the RF was estimated by mapping the classical receptive field (CRF) using a standard reverse-correlation paradigm (DeAngelis *et al.*, 1993; Ringach & Shapley, 2004). Dark and light squares of 0.1° width and 50% Michelson contrast were used as mapping stimuli. Stimuli were presented for ∼40 ms at 144 locations on an equally spaced grid covering an area of 1.2 × 1.2° in visual space. Stimulus order within the reverse correlation sequence was pseudorandomized. This procedure results in CRF estimates which are largely equivalent to the minimum response field (mRF; Barlow *et al.*, 1967; Maffei & Fiorentini, 1976). Following determination of the CRF centre and size, we determined orientation and spatial frequency tuning properties by using a reverse-correlation technique. Stimuli were 336 circular patches of static sinusoidal gratings (1.0° diameter) varying in orientation (12 orientations 0–165°), spatial frequency (1, 3, 5, 7, 8, 9 or 10 cycles/°) and phase (0, 0.5π, π, 1.5π). Each grating was presented for ∼63 ms (seven frames at a refresh rate of 110 Hz) in a pseudorandomized order.

After characterizing the basic response properties, we measured the spatial integration properties by presenting circular patches and annuli of static sinusoidal grating. Patches had one of nine different outer diameters (0.1, 0.25, 0.5, 0.75, 1.0, 1.5, 2.0, 3.0 or 4.0°). Annuli had a fixed outer diameter of 8.0° and one of nine different inner diameters (0.1, 0.25, 0.5, 0.75, 1.0, 1.5, 2.0, 3.0 or 4.0°). The monkeys began each trial by fixating on the fixation spot. After 500 ms a sequence of three stimuli was presented, each shown for 500 ms, separated by a gap of 500 ms. The selection of the stimulus type (size, and patch or annulus) and their order of presentation within a trial was pseudorandomized. On finishing a complete series of three stimuli (3 s fixation time) the monkey received a juice reward.

Data analysis

Before processing the LFP signal we removed 50 Hz line noise. To do so, we fitted the phase and amplitude of a 50 Hz sine function to the LFP signal of each trial separately. The resulting fitted sine curve was then subtracted from the signal. Afterwards the LFP signal was low-pass filtered (third-order Butterworth filter) with a cutoff frequency at 150 Hz. All analyses were performed using functions provided by the Matlab computing environment (Matlab 6.5; Mathworks, Natick, MA, USA).

Shortly after stimulus onset MU and LFP signals are usually characterized by a transient followed by a more sustained signal. Hence, two epochs (corresponding to the transient and sustained period) can be defined to analyze the spatial summation properties of the LFP and the MU signal. The baseline activity for both signals was determined in a time window of 300–0 ms before stimulus onset. As we were mainly interested in LFP gamma-band activity in the context of this paper, and this was most prominent during the sustained response period (see Results section), we focused exclusively on a time window ranging from 200 to 500 ms after stimulus onset. MU activity was defined as the average firing rate in the corresponding time window. To make sure that our results were not corrupted by transients of the early visual response we repeated all analyses using a time window from 300 to 500 ms after stimulus onset. Using that analysis window did not alter any of the results presented here, and we thus present data from the 200 to 500 ms period. To quantify the LFP activity we calculated the power spectrum in the baseline (BPS) and in the response window (RPS) of each trial via discrete Fourier transformation. The standard deviation (SD) of the baseline power spectrum (BPS_{SD}) was obtained from all the power spectra of the baseline window of trials of all stimulus conditions. The stimulus-induced power spectrum of each trial was expressed as the *z*-score of BPS:

$$PS_z = \frac{RPS - BPS}{BPS_{SD}} \quad (1)$$

The population stimulus specific power spectrum was calculated by averaging all PS_Z of a particular stimulus.

LFP responses were defined as the mean power in a specific frequency band. We divided the full spectrum (0–150 Hz) into four sections for separate analysis. The first three sections comprise the classical alpha (8–12 Hz), beta (12–25 Hz) and gamma (25–100 Hz) bands. The gamma band which is often deemed perceptually or behaviorally significant in visual studies (Eckhorn *et al.*, 1988; Gray *et al.*, 1989; Fries *et al.*, 2001) was constricted to the low gamma band (30–60 Hz) for a more detailed analysis of spatial summation parameters. The fourth band ('fast'; 100–150 Hz) covers frequencies faster than the classical gamma band. Different bands were used as they can differentially reflect tuning properties or perceptual state of the animal (Kayser & Konig, 2004; Henrie & Shapley, 2005; Wilke *et al.*, 2006).

To analyze the temporal structure of the MU spiking activity we computed autocorrelograms (ACGs) of MU spike trains in the sustained response window. For each stimulus-specific ACG we used spikes of all trials in the specific stimulus condition. The widths of the histograms were 200 ms (± 100 ms) with a binwidth of 1 ms. We corrected ACGs in three steps to allow for comparison between experiments and stimuli. First, ACGs were normalized by dividing each bin by the value of the central bin (i.e. the total number of spikes for that stimulus condition). Second, we replaced the central bin by the mean of the two adjacent bins. Third, to eliminate the offset of the ACG that was introduced by the summation process we subtracted the mean of all ACG bins. ACGs that were computed from < 50 spikes total were discarded from further analysis. The temporal structure of the spike trains was then quantified by calculating the power spectrum of the ACG. To estimate the significance of spectral peaks in the ACG we employed a Monte Carlo simulation procedure (Friedman-Hill *et al.*, 2000). Therefore the spikes in the response window of each trial were randomly reallocated within the spike train assuming a refractory period of 1 ms. Then we recalculated the ACG and its power spectrum as described above. This was repeated 500 times creating a population of 500 simulated power spectra for each stimulus condition. We regarded a peak in the power spectrum as significant if its amplitude exceeded the maximum amplitude as the same frequency in the simulated power spectra (i.e. $P < 0.002$).

Model fit

Parameter of spatial summation of the MU and of the LFP signal were obtained from theoretical models fitted to the experimentally derived data. A regularly used model to describe spatial summation properties in V1 cells is the so-called difference of Gaussian (DOG) model (Sceniak *et al.*, 1999; Roberts *et al.*, 2005, 2007).

The fitted function is of the form

$$R = K_e(1 - \exp^{-(2y/a)^2}) - K_i(1 - \exp^{-(2y/b)^2}) \quad (2)$$

where R corresponds to the model's response to a stimulus of size y, K_e corresponds to the excitatory component amplitude (the summation gain), a corresponds to the size constant of the excitatory area (referred to as 'summation area'), K_i corresponds to the inhibitory component amplitude (the suppression gain) and b is the size constant of the inhibitory area (referred to as 'suppressive area'). The model parameters were derived by minimizing the χ^2 error between the experimental data and the model predictions. The χ^2 error was defined as

$$\chi^2 = \sum_i \frac{(e_i - o_i)^2}{\sigma_i^2} \quad (3)$$

where e_i and o_i were the model's expected and the observed mean response for the ith stimulus and ${\sigma_i}^2$ was the observed variance of the response.

Suppression index

For each MU and LFP we calculated the suppression index (SD) according to:

$$\mathrm{SI} = \frac{R_{\max} - R_{\mathrm{largest}}}{R_{\max}} \quad (4)$$

where $R_{\max}$ corresponds to the maximum response (whichever stimulus triggered it) and R_{largest} corresponds to the response that occurred for the largest patch stimulus.

Contribution of different RF parts to the strength of oscillatory LFP activity

To determine the relative contribution of different parts of the classical and nonclassical receptive field to the spectral power in the gamma range, we performed a normalization of the LFP response. The weighted contribution of a stimulus area to the LFP response at increasing distances from the RF centre was defined as

$$R_{\mathrm{norm}} = \mathrm{d}R_{\mathrm{Stim}} \frac{S_{\mathrm{RF}}}{\mathrm{d}S_{\mathrm{Stim}}} \times \frac{1}{R_{\mathrm{RF}}} \quad (5)$$

where $\mathrm{d}R_{\mathrm{Stim}}$ was the increase in LFP gamma power (z-score) that occurred when the stimulus patch increased, $\mathrm{d}S_{\mathrm{stim}}$ was the increase in stimulus size, S_{RF} was the size of the MU receptive field (the summation area of the MU activity was taken as an alternative measure) and R_{RF} was the strength of gamma power for a stimulus confined to the MU receptive field (summation area). This measure is equivalent to a measure previously used for a similar purpose (Bauer *et al.*, 1995).

Results

We recorded a total of 123 recording sites in two monkeys (monkey FR, $n = 99$; monkey HU, $n = 24$). We typically started recording neuronal data as soon as we monitored well defined spiking activity following electrode insertion through the dura. Hence most recordings were presumably from layers 2/3. The median eccentricity of RF centres was 4.71° (horizontal range, −3.76° to +2.30°; vertical range, −6.21° to −1.59°). The median RF diameter was 0.49°.

Our stimuli (static sinusoidal gratings) often elicited strong oscillatory responses in the LFP signal. Figure 1 shows the LFP and MU responses to gratings and annuli of three different diameters for an example recording site. The LFP response was characterized by two components. The first was the visual evoked potential (VEP), which is a voltage change of relatively high amplitude and low frequency (∼10 Hz). The VEP dominated the early LFP response from ∼30 to 130 ms after stimulus onset. Even stimuli that did not fall into the CRFs of the recorded MU cluster elicited a VEP in the LFP signal, e.g. a grating annulus of adequate diameter (Fig. 1H). This reflects the fact that the LFP emerges from a broader integration of neuronal signals than the spiking MU signal. The second component of the LFP response consisted of sustained oscillations of a higher frequency than the VEP. These oscillations emerged in the late part of the LFP response (from ∼200 ms after stimulus onset onwards), were often visible in single-trial data (e.g. Fig. 1C) and had a dominant frequency in the gamma range of ∼35–45 Hz. Figure 1 also shows that gamma frequency LFP oscillations increased with increasing stimulus size (Fig. 1A–D) while they decreased with increasing annulus diameter (Fig. 1F–I). The simultaneously recorded MU activity is shown below

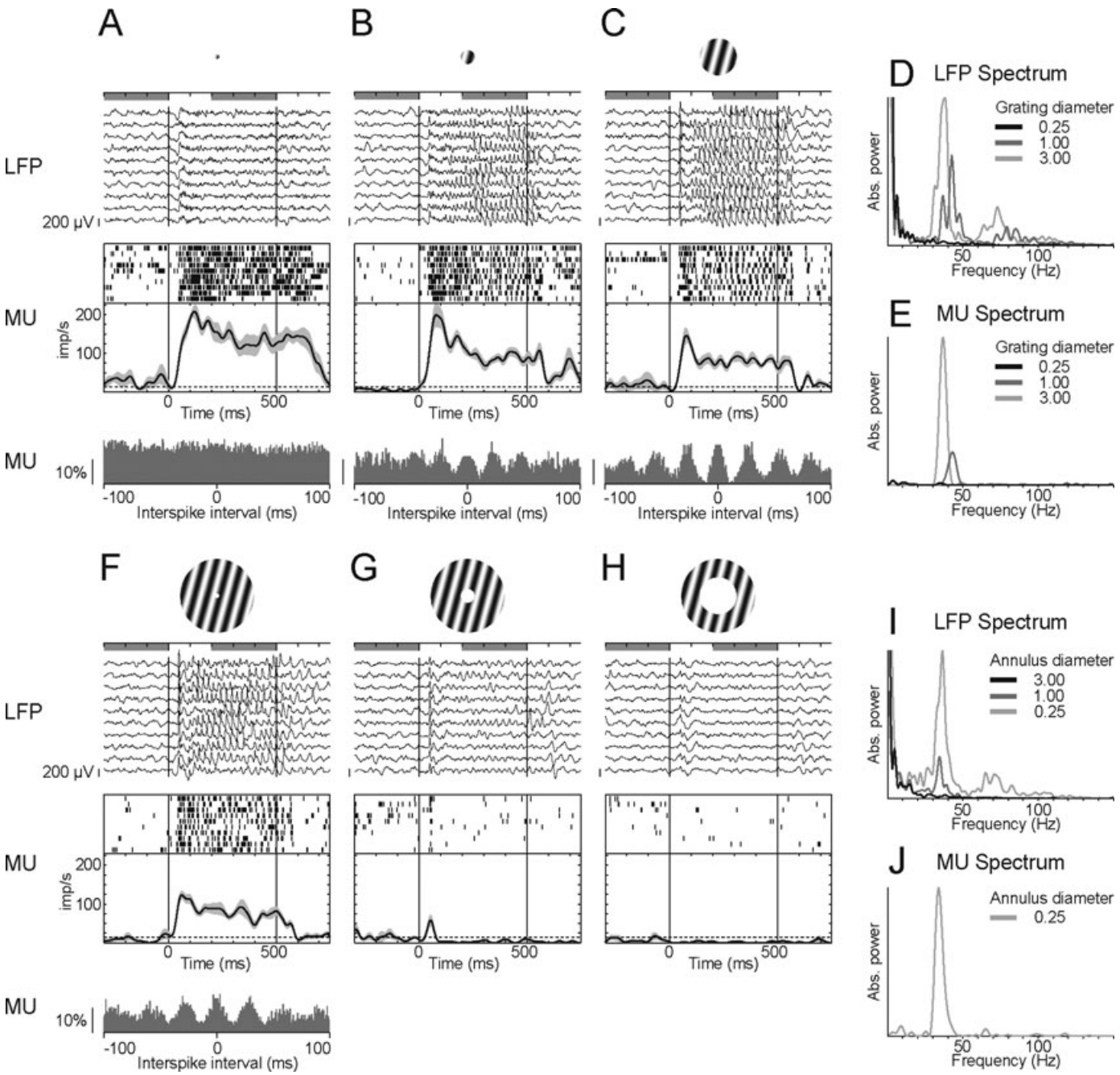

FIG. 1. Neuronal responses at an example recording site. The figure shows MU and LFP activity to grating stimuli of three different sizes. (A–C) Responses to circular grating patches with a diameter of 0.25, 1 and 3°. (F–H) Responses to grating annuli with an annulus diameter of 0.25, 1 and 3°. LFP traces of single trials are shown on top of each panel (high-pass-filtered at 8 Hz for convenience of illustration). The middle panels show raster and mean spike density plots of spiking activity (sigma 10 ms, SE as gray shaded area, mean spontaneous activity as dashed line). The autocorrelogram (200 ms width, 1 ms bins) is shown at the bottom of each panel. Vertical lines indicate the stimulus presentation window, 0–500 ms. Gray horizontal bars on top of each panel indicate the baseline (−300 to 0 ms) and the analysis window (200–500 ms). (D and I) The average power spectrum of the LFP activity in the analysis window. (E and J) The power spectrum of the autocorrelogram.

the LFP traces in Fig. 1. Spiking activity generally decreased with increasing stimulus diameter (Fig. 1A–C), a testament of surround suppression. However, despite this decrease in firing rate, the ACGs revealed that spiking activity started to oscillate at ∼ 35–45 Hz when large stimuli were presented (Fig. 1E), while such oscillations in the MU activity were usually absent for stimuli confined to the CRF (see ACG at the base of Fig. 1A).

The increase in oscillatory strength in the LFP with increasing stimulus diameter for the population of recording sites is shown in Fig. 2. Figure 2B shows the average spectral power in the LFP pooled across both monkeys for three different stimulus sizes. Oscillations in the gamma range increased as stimuli increased, and this was the case in both monkeys. From Fig. 2, two additional main findings are evident: (i) the dominant oscillatory frequency seemed to change with

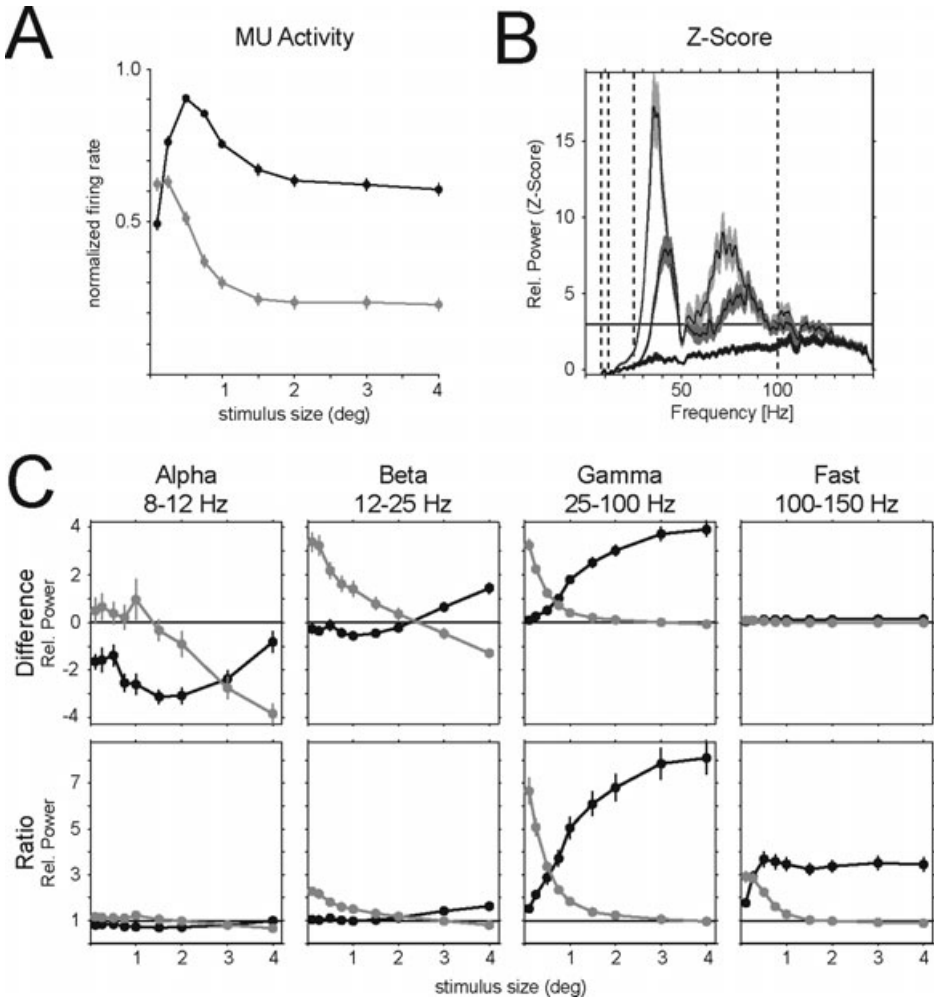

FIG. 2. (A) Average MU activity (pooled across monkeys; error bars denote SE) plotted as a function of stimulus size (black, patches of grating; gray, annuli of grating). (B) Stimulus-modulated LFP spectra averaged across all recording sites and monkeys (gray shading denotes SE) for three stimulus diameters (light gray, 3°; medium gray, 1°; dark gray, 0.25°). Only the power of frequencies > 8 Hz are plotted. *Z*-score was computed as the difference between baseline and stimulus spectrum from every single trial, divided by the SD of the baseline spectrum across trials. Solid line indicates a *z*-score level of 3. Vertical dashed lines indicate the borders of classical frequency bands (α, β and γ bands). (C) Average power (pooled across monkeys; error bars denote SE) in the four frequency bands (α, β, γ and fast bands) plotted as a function of stimulus size. Upper row shows the difference in power between the spectrum during stimulus presentation and the baseline spectrum. Lower row shows the response gain as the ratio between the spectrum during stimulus presentation and the baseline spectrum. Only experiments showing a significant modulation of the spectrum by stimulus presentation (two-way ANOVA, $P < 0.01$) were included (black, patches of grating; gray, annuli of grating).

increasing stimulus size; and (ii) the LFP exhibited multiple peaks. We will return to these two features in more detail later. Figure 2C shows the spectral power in different frequency bands across the population of recording sites for the different stimulus and annulus sizes relative to the baseline (prestimulus) condition. For all frequency bands the spectral power increased as the stimulus diameter increased (black curves), and it decreased with increasing inner annulus diameter. The largest effect of stimulus (annulus) size on spectral power was found for the low gamma range. Figure 2A shows the corresponding graphs for MU spiking activity. It demonstrates that spiking activity was inhibited at the population level when stimuli were presented that extended beyond the summation area.

The example shown in Fig. 1 suggested that the oscillation frequency depended on stimulus size. Figure 3 shows the spectral power in the low gamma band (25–60 Hz) for the population of recording sites for the different stimulus patches (Fig. 3A, monkey FR; Fig. 3C, monkey HU) and the different annuli (Fig. 3B, monkey FR; Fig. 3D, monkey HU). For both monkeys we found a monotonic decrease in oscillation frequency with increasing stimulus patch size, combined with an overall increase in spectral power. To quantify these findings for the different recording sites we determined the peak frequency for each recording that occurred in the low gamma range for each stimulus patch (annulus) and fitted a linear regression to the data with the patch size (annulus diameter) as the independent variable. The distribution of the resulting regression slopes is shown separately for both monkeys in Fig. 3I–L. The median regression slope (only significant regressions were included) for increasing stimulus patches was −2.95 (monkey FR) and −1.58 (monkey HU). Both median slopes were significantly different from zero ($P < 0.001$, monkey FR; $P < 0.05$, monkey HU; sign test). In other words, the frequency decreased by a median of 2.95 Hz for monkey FR (1.58 Hz for monkey HU) for every degree the stimulus increased in size (within the range tested). A similar result was found when the oscillation frequencies of the MU activity were analyzed. For monkey FR we found significant regressions in 14 MU recordings (distribution not shown). The median was −3.03 ($P < 0.001$, sign test) and the distribution of slopes was not different from the LFP data (Fig. 3I; $P = 0.301$, Wilcoxon signed-rank test). The regressions of LFP

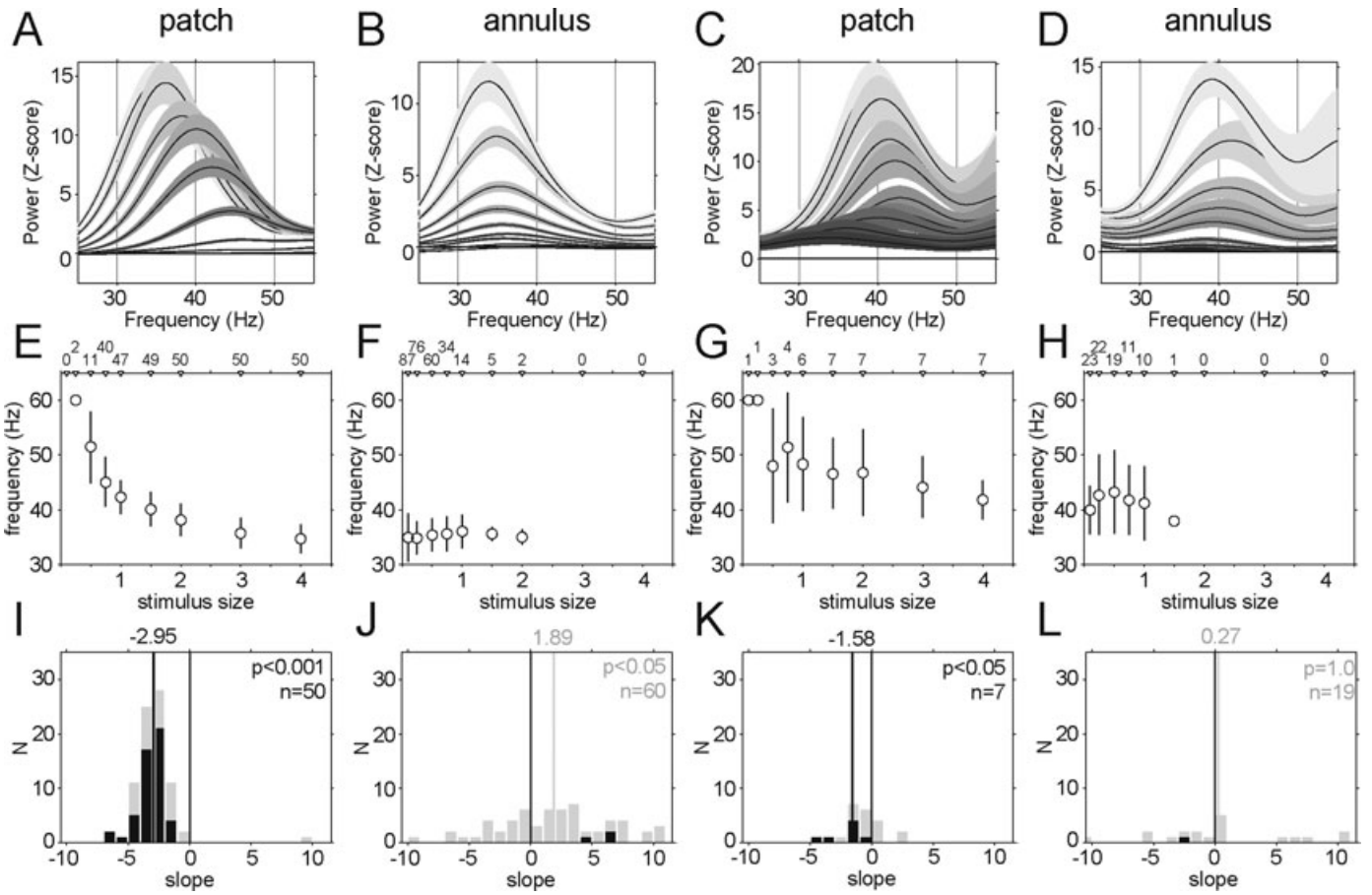

FIG. 3. Oscillation frequency as a function of stimulus size. Left and right two columns show data from monkeys FR and HU respectively. Data of grating patches (annuli) are shown in the first (second) and third (fourth) columns. (A–D) Average smoothed LFP power spectra in the low gamma range for nine grating sizes (A and C; dark to light gray indicate increasing patch diameter) and annuli (B and D; dark to light gray indicate decreasing annulus diameter). (E–H) Oscillation frequency as a function of stimulus size. Data are shown as mean ± SD of experiments with significant (z-score > 3) oscillations. Number of experiments contributing to the mean are denoted on top of the figures above each data point (inclusion was determined by the presence of a significant peak in the spectrum, i.e. z-score > 0. (I–L) Histograms of the distribution of slopes. Slopes were obtained by calculating a regression of grating (I and K) and annulus (J and L) diameter on the peak frequency in the low LFP gamma-band range. Black and gray bars and letters refer to significant ($P < 0.05$, black) and all (gray) regressions. The dashed line and number at the top indicate the median of the distribution.

gamma peak frequency as a function of annulus size were rarely significant for a single recording site ($P < 0.05$, Fig. 3J and L; $n = 3$ in monkey FR, $n = 1$ monkey HU). However, from Fig. 3B and D it seems that increasing the annulus diameter did not result in the same systematic change in the LFP oscillation frequency. For monkey FR the median slope of all calculated regressions (including nonsignificant regressions) was smaller than the concurrent decrease in frequency with increasing stimulus diameter, although the distribution was nevertheless different from zero (median = 1.89, $P < 0.05$; Fig. 3J). For monkey HU the median change of 0.27 Hz/° for the annuli was also smaller than the corresponding change with patch stimuli, and this distribution was not significantly different from zero ($P = 1.0$; Fig. 3L).

One of the main topics of this paper was to determine whether inhibitory processes (which are likely to be involved in surround suppression) can be related to features of the oscillatory activity seen in the LFP. Surround suppression in the context of spatial integration in primate V1 is well established. Neurons usually increase their firing rate with increasing stimulus size and somewhat reduce their firing rate when stimuli start to encroach into the suppressive surround (Carandini & Heeger, 1994; Sceniak *et al.*, 1999; Cavanaugh *et al.*, 2002; Levitt & Lund, 2002; Roberts *et al.*, 2005). To quantify the strength of suppression in our data we calculated the suppression index for each recording site for the MU and the LFP activity in the low gamma band (see Materials and methods). Our MU data replicated the well established phenomenon of surround suppression. Eighty-four MU sites (65%) showed a significant reduction in responses to the largest grating patches. Their median suppression index was 0.46 (Fig. 4C). Most MU sites exhibited their peak activity at a stimulus size of 0.5° diameter (Fig. 4A) and showed reduced activity when stimuli of ≥ 1° diameter were used. Conversely, most LFP recordings exhibited maximal oscillatory power in the gamma band at the largest stimulus tested (4° diameter; Fig. 4B). Most LFP recordings did not show any evidence of suppression, and the distribution of suppression indices peaked at a value close to zero (Fig. 4D). The suppression indices between MU and LFP data were not correlated ($r = 0.08$, $P = 0.349$) and, importantly, their distributions differed significantly between MU and LFP data ($P < 0.001$, signed-rank test; Fig. 4D).

Spatial integration properties in V1 neurons are well described by DOG models (Sceniak *et al.*, 1999, 2001; Roberts *et al.*, 2005, 2007), although Ratio of Gaussian models have also been proposed (Cavanaugh *et al.*, 2002). Both models assume that the RF of V1 neurons is composed of an area from which excitatory inputs are

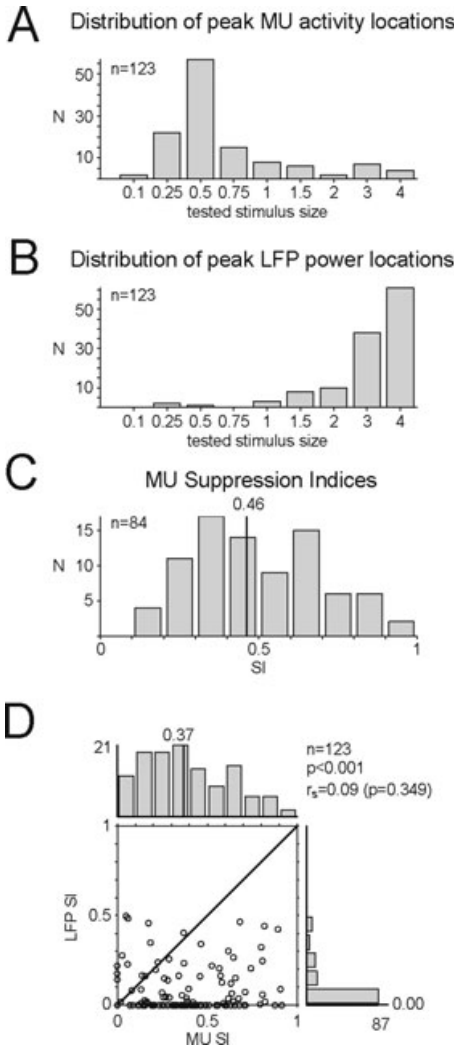

FIG. 4. Comparison of surround suppression in the MU and LFP response. (A) Distribution of stimulus sizes eliciting the maximal response in MU unit spiking activity. (B) Distribution of stimulus sizes eliciting the maximal response in LFP low gamma activity. (C) Distribution of the SI for all significantly modulated MUs. The solid vertical line indicates the median SI of 0.46. (D) Pairwise comparison of the distribution of all SIs calculated for MU and LFP activity. Vertical lines in histograms indicate the medians for MU and LFP SIs. These were significantly different ($P < 0.001$, Wilcoxon signed-rank test; r_s is the Spearman rank correlation coefficient).

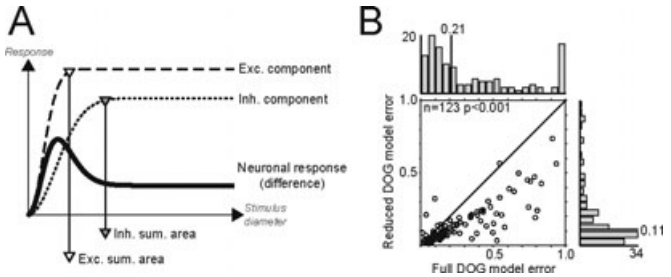

FIG. 5. (A) DOG model used to fit the MU responses. The neuronal response (black solid line) emerges from subtracting a wide Gaussian mechanism (inhibitory component, dotted line) from a narrower Gaussian mechanism (excitatory component, dashed line). The parameter of the fitted model yielded the extent of the summation and suppression area. (B) Comparison of the normalized χ^2 error (χ^2_N) resulting from fitting the full DOG model (abscissa) and the reduced DOG model (ordinate) to the LFP responses. Fitting the reduced model produced significantly lower χ^2_N values (Wilcoxon signed-rank, $P < 0.001$). Lines in the distribution histograms indicate the medians.

received (the summation area), which has superimposed on it a larger area from where the neuron receives inhibitory inputs (the suppression area; Fig. 6A). The main assumption is that the excitation gain is stronger than the suppression gain, which is why excitation dominates when small stimuli are presented in the RF. We were interested in whether this model can be usefully applied to LFP gamma oscillation strength, and whether certain parameters of this model can be compared with the parameters obtained from MU. We fitted the DOG model to our MU and LFP gamma power data. As demonstrated in Fig. 4 (and Fig. 2C), suppression was rarely evident in LFP data, which suggests that a full DOG model is unnecessary to describe spatial summation-induced LFP gamma-power changes. To confirm this, we fitted each LFP recording with a full DOG model and a reduced model where the inhibitory gain was set to zero, and the size of the inhibitory area was arbitrarily fixed at 1 (this effectively eliminates the inhibitory component of Eqn 2; see Materials and methods). We then determined the goodness of fit for the full and the reduced model by comparing the normalized χ^2 error. We found that the normalized χ^2 error was generally lower for the reduced model when compared to the full model and this effect was highly significant ($P < 0.001$, Wilcoxon signed-rank test; Fig. 5B). We thus performed all additional analyses and comparisons based on the reduced DOG model for the LFP responses while we used the full model for the MU responses.

Examples of full DOG fits to MU data and corresponding reduced DOG fits to low-gamma LFP data from selected recording sites are shown in Fig. 6. The majority of recording sites showed spatial summation curves as shown in Fig. 6A and B. Summation curves in Fig. 6C and D show exceptional examples. In general, LFP gamma oscillations are not very pronounced until the stimulus has at least reached, if not exceeded, the preferred MU stimulus patch size. This suggests that inhibition from RF surround mechanisms may contribute strongly to the gamma oscillations of the LFP. To determine whether it is possible to relate specific features of the MU DOG parameters to parameters from the reduced LFP DOG fit on a recording site-by-recording site basis we compared the size of the MU suppression area to the size of the LFP summation area (Fig. 7C). Additionally, we compared the location of the maximum negative slope of the MU response to the location of the maximum (positive) slope of the LFP gamma response (Fig. 7D). Comparison was restricted to parameters that resulted from good DOG fits (χ^2 $P > 0.5$). Spatial DOG parameters $> 10°$ were considered outliers. We did not find a significant correlation between the size of the MU suppression area and the size of the LFP summation area ($r = 0.02$, $P = 0.805$; Spearman rank correlation). The LFP 'summation' area (median 2.36) was significantly larger than the MU suppression area (median 1.80; Fig. 7C; $P < 0.001$, Wilcoxon signed-rank test). We equally did not find a correlation between the locations where the above-mentioned slopes were maximal (Fig. 8D; $r = 0.03$, $P = 0.763$, Spearman rank correlation). However, the median slope locations were fairly similar for the two measures (LFP slope, 0.84; MU slope, 0.78) and they were not significantly different from one another (Fig. 7D; $P = 0.091$, Wilcoxon signed-rank test), although there was a trend towards significant differences.

As evident from Fig. 6B and D, spatial summation properties of MU and LFP data were often similar when annuli were presented. MU and gamma-power LFP activity fell off rapidly with increasing inner annulus diameter. This suggests that LFP oscillations require

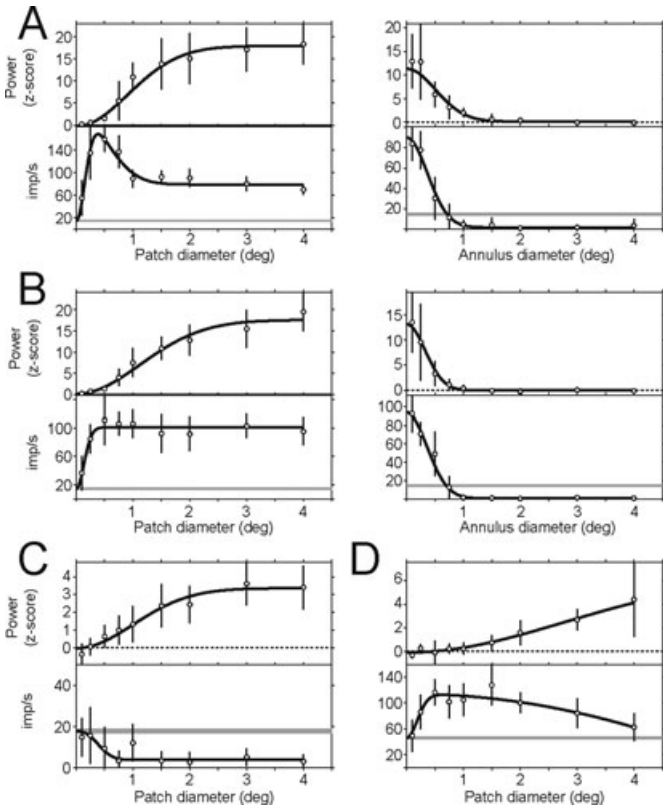

FIG. 6. Four examples of spatial summation in MU and low gamma (25–60 Hz) LFP responses. Data points show the mean ± SD of the MU (lower curves) and LFP (upper curves) responses. Solid lines show the DOG model fitted to the data. Examples shown in A and B (left, responses to patches; right, responses to annuli) were representative of the majority of recording sites. (A) Stimuli extending beyond the CRF induced strong suppression of MU activity while LFP gamma power increased asymptotically. (B) MU activity showed an asymptotic increase with stimulus size without suppression. Similarly, LFP gamma power increased with stimulus size as well, albeit at a slower rate. (C) Rare example of an MU inhibited by patches of circular gratings. The corresponding LFP gamma power showed the typical increase. (D) Rare example of a slow developing suppression of MU activity along with an equally slow increase in gamma power.

excitatory local drive in conjunction with the inhibitory drive from the surround. To compare how the LFP power depends on local excitatory drive we calculated the correlation of the Gaussian widths for the annulus MU and LFP data fits. Figure 7E shows these comparisons. We found a modest but significant correlation between the two parameters ($r = 0.28$, $P < 0.01$, Spearman rank correlation), which confirms that the strength of gamma power in the LFP requires the CRF of simultaneously recorded MU activity to receive strong excitatory drive. Moreover, the negative maximum slope locations were also similar and significantly correlated (Fig. 7F; $r = 0.33$, $P < 0.001$, Spearman rank correlation).

We were interested in determining which part of the RF and the RF surround contributed most to local gamma-frequency LFP oscillations. To investigate this we performed a normalization procedure identical to what has previously been used for cat area 17 and 18 data (Bauer *et al.*, 1995). The procedure determines the increase in gamma power induced by a given increase in stimulus size relative to the gamma power induced by stimulation of the receptive field only, plotted for the location where the stimulus increase occurred (see Materials and methods). The results are shown in Fig. 8. The figure shows that the largest increase in gamma power (per area of stimulation) occurred when stimuli started to infringe on the surround of the receptive field. The influence was maximal when stimuli had a size of 1°, and it fell off with increasing distance from the RF centre. This was the case whether the minimum response field (not shown) or the summation area were used as the basis for the normalization procedure (Fig. 8B). It demonstrates that the strongest determinant of gamma power strength is stimulation of the near (inhibitory) surround of neurons. However, this is only the case if the RF centre is also stimulated, as demonstrated in Fig. 8C. The figure shows the equivalent normalization procedure for the annulus stimuli, demonstrating that the largest decrease in gamma power with increasing annulus diameter occurred for very small annulus diameters. Thus, sparing even small parts of the RF can result in a substantial reduction in induced LFP gamma power.

Discussion

Our results show different spatial summation signatures in MU and LFP activity. While MU activity showed well established centre–surround suppression characteristics, spectral power in the gamma (and other) frequency bands increased monotonically with increasing stimulus size. The largest relative increase occurred when the immediate surround of the receptive field was stimulated. While stimulation of the receptive field surround was a necessary condition to induce strong gamma oscillations, it was not sufficient on its own. Gamma oscillations in the LFP equally required the receptive field of the simultaneously recorded MU activity to be stimulated. We will first discuss these results in relation to recent studies investigating visual tuning characteristics of LFPs. We will then discuss our findings in relation to mechanisms of gamma oscillation generation and in relation to perceptual binding. We will finally discuss how these findings could relate to interpretation of human fMRI BOLD signals.

Visual tuning properties of LFPs

A variety of recent studies have investigated the tuning properties of LFPs. A study most closely linked to ours has investigated spatial integration properties of MU and LFP gamma activity in area 17 and 18 of the anesthetized cat (Bauer *et al.*, 1995). In line with our finding the authors found that the LFP and MU gamma power increased with increasing stimulus size, while MU spiking frequency in their study exhibited moderate signs of suppression. Despite this overall similarity there are notable differences between their results and ours. Bauer *et al.* (1995) found only a moderate increase in oscillatory drive when increasing the stimulus from the RF size to a size much bigger than the RF. Conversely, we found that the largest increase occurred when stimuli larger than the RF size were presented. Bauer *et al.* (1995) concluded from their results that the largest oscillatory drive is generated by neurons that contribute to RF responses themselves, while in our study it was the immediate surround that had the largest impact on oscillation strength. Also, Bauer *et al.* (1995) found only limited evidence for surround suppression in their MU activity, particularly for area 17, while surround suppression was a prominent feature in our sample. There are a variety of possible explanations for these discrepancies. Firstly, Bauer *et al.* (1995) used an anesthetized preparation, and the anesthetic used (halothane) increases tonic inhibitory drive (Mody *et al.*, 1991; Jones & Harrison, 1993). As inhibitory interneurons are assumed to be a key mediator of gamma oscillations (e.g. Traub *et al.*, 1996b; Whittington & Traub, 2003; and see below), this tonic inhibitory drive could result in gamma oscillations for stimuli that would otherwise only yield small oscillations. Tonic inhibitory drive due to anesthesia may also account

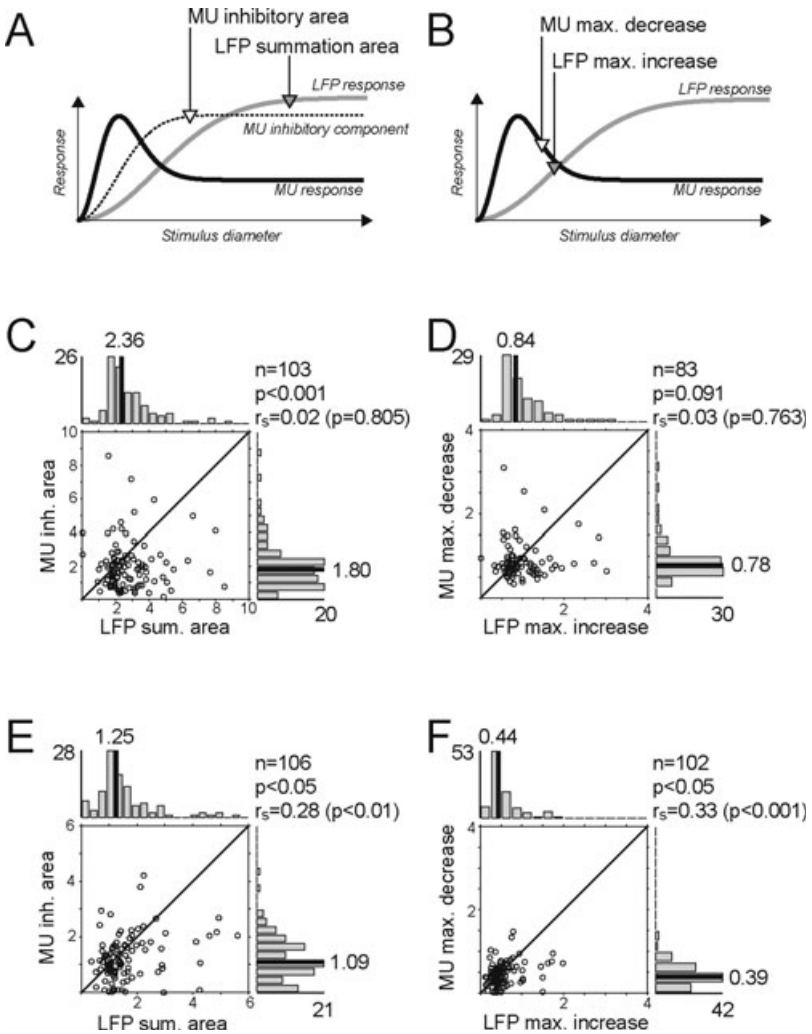

FIG. 7. Comparison of MU and LFP spatial summation parameter. (A and B) Sketches of the two types of parameter extracted from the model fits to responses to different sizes of grating patches. (A) White arrow denotes the width of the Gaussian representing the inhibitory component of the DOG fit to the MU response (dashed line). Gray arrow shows the extent of the Gaussian fitted to the LFP data (see text). (B) White arrow shows the stimulus size exhibiting the strongest increase in MU suppression (minimum slope). Gray arrow shows the stimulus size when increase in LFP gamma power is maximal (maximum slope). (C and D) Scatter plots of spatial parameter derived from stimulation with patches of grating (*x*-axis, LFP parameter; *y*-axis, MU parameter; solid black lines in histograms, median of each distribution; p-value, Wilcoxon signed-rank test; r_s, Spearman rank correlation coefficient). (E and F) Scatter plots of spatial parameter derived from the model fits to responses to grating annuli (plots are the same style as in C and D).

for the relatively small surround suppression in spiking activity of the data of Bauer *et al.* (1995). A further possible source of the discrepancies between their and our data is the size of the stimuli used. The smallest stimulus size in their sample was 2.5° wide which, for area 17 (at an eccentricity of 2–10°), may have exceeded the average classical receptive field and thus already encroached upon the RF surround (Wilson & Sherman, 1976). It may be a combination of these factors which led Bauer *et al.* (1995) to suggest that the largest contribution to gamma oscillations arises from the network that directly supports RF responses, while we found that the immediate surround contributes the most (relative to each mm^3 of cortical tissue that is activated by a visual stimulus).

We also found a decrease in oscillation frequency with increased stimulus size. To the best of our knowledge, reports about changes in oscillation frequency depending on visual stimuli are rare. A reduction in gamma oscillation frequency has been reported for V1 when overall neuronal excitability is increased by activation of the midbrain reticular formation (Herculano-Houzel *et al.*, 1999). Friedman-Hill *et al.* (2000) found that oscillation frequencies increase with moving compared to stationary stimuli. A conference abstract by Woelborn *et al.* Woelbern *et al.* (1994) reported a dependence of oscillation frequencies on stimulus size and velocity, but did not supply sufficient information to allow for a detailed comparison to our data. Other recent studies have mostly assessed the tuning characteristics of LFP spectral power. Most of these reports have concluded that tuning to visual features is strongest for the LFP gamma band (Friedman-Hill *et al.*, 2000; Frien *et al.*, 2000; Henrie & Shapley, 2005; Liu & Newsome, 2006). Based on the similarity of LFP and MU tuning it has been argued that the gamma-band LFP reflects the summed electrical signal of about one cortical column i.e. ~1–2 mm in diameter around the electrode tip (Liu & Newsome, 2006). While this may be the case when restricted stimulus sizes were used, our data showed that much larger cortical areas can contribute to the strength of gamma-band LFP (for further discussion see below), provided the stimulation engages the inhibitory interneuron network.

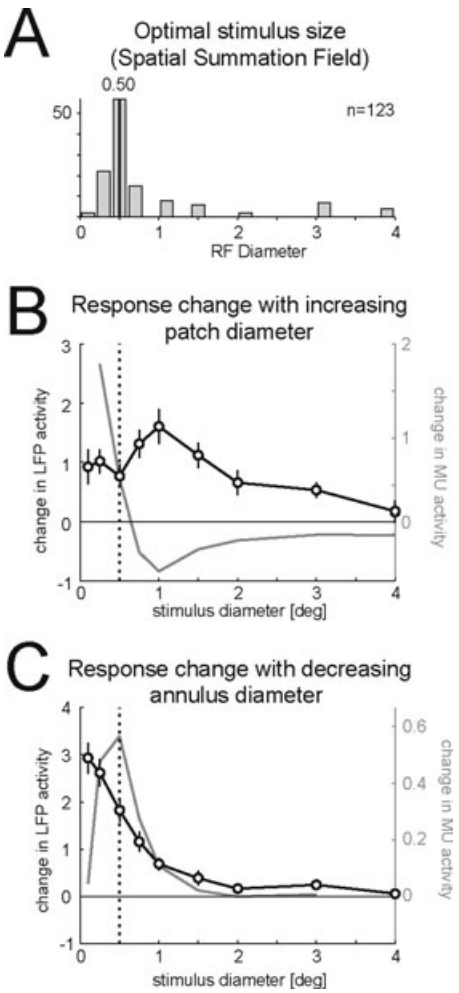

FIG. 8. Relative increase in LFP gamma power in relation to the increase (decrease) in stimulus size. (A) Distribution of stimulus sizes eliciting maximum MU activity (Spatial Summation Field). Values were derived from the DOG-model fits and were used as normalization references (median value denoted by vertical solid line) for the data in B and C. (B) LFP gamma power increase relative to increase in patch diameter and normalized to the response elicited by stimuli of the size of the Spatial Summation Field. Change in MU activity with increasing stimulus diameter (first derivative of Fig. 2C) is shown in gray. (C) LFP gamma power increase relative to decrease in annulus diameter and normalized to the response elicited by stimuli of the size of the spatial summation field. Change in MU activity with decreasing annulus diameter (first derivative of Fig. 2C) is shown in gray.

Underlying architecture that mediates gamma oscillations

While stimulation of the receptive field centre was necessary to induce strong gamma oscillations it was not a sufficient condition. When the receptive field surround was covered by ~0.5° of visual angle (i.e. a stimulus of 1° diameter total) we found the largest increase in gamma oscillation per area of visual stimulation (see Fig. 8), suggesting that the immediate V1 centre–surround circuitry has the strongest impact on gamma oscillations. The well studied cortical magnification factor in V1 allows estimation of the extent of cortical tissue mediating this effect. Most of our recordings were at an eccentricity of 4.71° (median). The V1 magnification factor for that eccentricity is ~2.1 mm/° according to Dow *et al.* (1981), ~2.4 mm/° according to Daniel & Whitteridge (1961) and ~2.7 mm/° according to Tootell *et al.* (1988). Taking the average value of 2.4 mm/° as a base value, it means that the maximum oscillatory drive occurs from locations that are between 0.6 and 1.2 mm away from the recorded neurons [the maximum oscillatory increase per area stimulated occurred for stimuli that increased from 0.5° diameter (radius of 0.25°, generally just covering the receptive field) to stimuli that had a diameter of 1.0° (encroaching on the inhibitory surround), i.e. a radius of 0.5°]. This suggests that the main gamma oscillatory drive occurs when stimuli extend over more than a single cortical hypercolumn, which in V1 is assumed to be at least 1 mm in diameter (Hubel & Wiesel, 1974; Swindale, 1991).

Structural basis for LFP gamma oscillations: lateral or feedback connections?

Lateral connections in V1 extend beyond distances that are necessary to cover the cortical area from which strong gamma oscillations are induced (McGurie *et al.*, 1991; Das & Gilbert, 1995; Angelucci *et al.*, 2002). Thus, the main oscillatory drive for gamma oscillations may arise from the local surround within V1 itself. While early models have assumed that gamma oscillations are triggered through increased coupling within the pyramidal cell network (Bush & Douglas, 1991; Gray & McCormick, 1996), recent modelling, *in vitro* and *in vivo* studies point towards inhibitory interneurons as the main source of gamma oscillations (Traub *et al.*, 1996b; Wang & Buzsaki, 1996; Brunel & Wang, 2003; Buzsaki & Draguhn, 2004; Tiesinga & Sejnowski, 2004). In particular, electrically coupled fast-spiking GABAa basket cells seem to play a key role (Galarreta & Hestrin, 1999; Tamas *et al.*, 2000; Amitai *et al.*, 2002; Whittington & Traub, 2003; Hasenstaub *et al.*, 2005; Hestrin & Galarreta, 2005). Large basket cells are the primary source of lateral inhibition across cortical columns (Markram *et al.*, 2004), and would thus be a possible source that mediates the increase in gamma power when neighboring columns are visually stimulated. However, it is equally possible that lateral excitatory connections target inhibitory interneurons that represent the RF location itself, which in turn contribute to increased gamma power when large parts of the visual field are activated. The conduction delay of long-range lateral interactions of ~0.2 m/s (Grinvald *et al.*, 1994; Bringuier *et al.*, 1999) means that cortical distances of 1–2 mm are traversed in 5–10 ms, which would be within a single oscillatory cycle even if phase shifts would not be compensated for (Traub *et al.*, 1996a).

The above explanation does not account for the possibility that suppressive surround modulation is due to feedback from other areas, as suggested by a variety of studies (Angelucci *et al.*, 2002; Bair *et al.*, 2003). However, the feedback proposal also faces explanatory problems. Feedback would need to target inhibitory interneurons (feedback connections are mostly glutamatergic; Johnson & Burkhalter, 1994), but feedback has been shown to target mostly pyramidal cells while terminals on inhibitory interneurons are rare (Johnson & Burkhalter, 1994; Shao & Burkhalter, 1996, 1999). Thus, feedback would have to drive principal cells in V1 which in turn increases local inhibition through pyramidal–interneuron interactions. At this stage it seems futile to argue for an exclusive version of either lateral or feedback contributions to increased gamma LFP power. It is likely that both contribute to the spatial integration properties described herein, although feedback may have been more influential for gamma drive when larger stimuli of 2–4° diameter were presented.

In addition to an increase in gamma power with increasing stimulus size we also found a decrease in oscillation frequency. It has been proposed that oscillation frequency decreases for long-range interactions as conduction delays increase (Miller, 2007). Given that the size of our stimuli affected the activated neuronal pool size and thus the involvement of different ranges of neuronal interactions, the change in oscillation frequency may be a direct reflection of this increase in

conduction delays with cortical distance. At the same time modelling studies (Brunel & Wang, 2003) have shown that the frequency of oscillations is critically dependent on the number of excitatory cells in a network, where the main oscillation drive arises from electrically coupled interneurons. As the larger stimuli excited additional pools of excitatory neurons, the reduction in frequency may have arisen from the increased pool of contributing principle cells, while the increased oscillatory drive may have arisen from an increased pool of active (and coupled) interneurons.

Oscillations and perceptual binding

Coupling between groups of neurons in the gamma frequency range has been proposed as a mechanism for perceptual grouping ('binding by synchrony'; BBS; Eckhorn *et al.*, 1988; Gray *et al.*, 1989; Freiwald *et al.*, 1995; Kreiter & Singer, 1996; Singer, 1999). Although we did not measure multiple cell ensembles at different electrodes simultaneously, our findings still bear on the topic. Many of the experiments testing the BBS hypothesis have quantified the strength of oscillation (or synchrony in some experiments) between simultaneously recorded neurons or sites when the RFs were stimulated with a single bar (object), and compared it to the strength of oscillations when the two site RFs were stimulated by separated bars (objects), e.g. Freiwald *et al.* (1995); Kreiter & Singer (1996). These studies found that gamma-frequency oscillations were stronger for the single-bar than the two-bar condition, which was taken as evidence supporting the BBS hypothesis. However, the single-bar condition is likely to invoke more inhibitory surround activation than the dual-bar condition. Our V1 data show that surround suppression in MU spiking activity was stronger for a single large circular grating than for a grating stimulus that covered the same (or even a larger) area, but that was interrupted by a small circular gap (unpublished observations), demonstrating that suppression is stronger for single extended stimuli. As the data presented here show that the strength of oscillations is related to the amount of surround suppression, increased oscillatory drive for single bar stimuli may simply be a reflection of differential activation of the inhibitory network and high levels of recurrent interactions in the network (Henrie & Shapley, 2005) rather than reflecting perceptual grouping (or binding). Such an interpretation would be compatible with recent studies in awake monkeys which failed to provide support for the BBS hypothesis (de Oliveira *et al.*, 1997; Thiele & Stoner, 2003; Roelfsema *et al.*, 2004; Palanca & DeAngelis, 2005) and in which the stimuli used were less likely to result in differential activation of the inhibitory network.

Signatures of inhibition in LFP and MU activity and its implications for fMRI BOLD studies

A variety of studies have highlighted the similarity between the LFP signal and the BOLD signal which is usually measured in fMRI experiments (Logothetis *et al.*, 2001; Logothetis, 2002; Kayser *et al.*, 2004; Mukamel *et al.*, 2005; Niessing *et al.*, 2005; Nir *et al.*, 2007). Most of these studies have reported that the LFP (particularly in the gamma range) is better correlated with the BOLD signal than single- or multiunit spiking activity (Logothetis *et al.*, 2001; Logothetis, 2002; Kayser *et al.*, 2004; Mukamel *et al.*, 2005; Niessing *et al.*, 2005; Nir *et al.*, 2007), unless neurons themselves exhibited high level of firing rate correlations (Nir *et al.*, 2007). These reports somewhat conflict with other studies that stress the good correspondence between firing rates and BOLD activity (Boynton *et al.*, 1996; Rees *et al.*, 2000). We show a dissociation between MU firing rates and LFP gamma power when large stimuli are presented which invoke strong inhibitory processes. Under these conditions LFP gamma power becomes maximal while firing rates are reduced. If BOLD activity was better correlated with the strength in gamma power, it would predict that centre–surround suppression or other processes that invoke significant amount of mutual inhibition should not be directly accessible by means of the BOLD signal, as this should rise proportionally with the LFP gamma power. However, a few studies have demonstrated that surround suppression results in reduced fMRI BOLD signal (Williams *et al.*, 2003; Zenger-Landolt & Heeger, 2003; Delicato *et al.*, 2006). This suggests that the coupling between BOLD and LFP depends on the specific stimulus conditions; it may break down when large inhibitory networks are involved, highlighting the need for additional studies to determine how the BOLD is related to neuronal activity under a variety of different network states.

Acknowledgements

The work was supported by the BBSRC (BBS/B/09325) and the Wellcome Trust (070380/Z/03/Z).

Abbreviations

ACG, autocorrelogram; BBS, binding by synchrony; BOLD, blood oxygen level-dependent; CRF, classical RF; DOG, difference of Gaussian; fMRI, functional magnetic resonance imaging; LFP, local field potential; mRF, minimum response field; MU, multiunit; RF, receptive field; SD, standard deviation; SI, suppression index; VEP, visual evoked potential.

References

Allman, J., Miezin, F. & McGuinness, E. (1985) Stimulus specific responses from beyond the classical receptive field: neurophysiological mechanisms for local-global comparisons in visual neurons. *Annu. Rev. Neurosci.*, **8**, 407–430.

Amitai, Y., Gibson, J.R., Beierlein, M., Patrick, S.L., Ho, A.M., Connors, B.W. & Golomb, D. (2002) The spatial dimensions of electrically coupled networks of interneurons in the neocortex. *J. Neurosci.*, **22**, 4142–4152.

Angelucci, A., Levitt, J.B. & Lund, J.S. (2002) Anatomical origins of the classical receptive field and modulatory surround field of single neurons in macaque visual cortical area V1. *Prog. Brain Res.*, **136**, 373–388.

Bair, W., Cavanaugh, J.R. & Movshon, J.A. (2003) Time course and time-distance relationships for surround suppression in macaque V1 neurons. *J. Neurosci.*, **23**, 7690–7701.

Barlow, H.B., Blakemore, C. & Pettigrew, J.D. (1967) The neural mechanism of binocular depth discrimination. *J. Physiol.*, **193**, 327–342.

Bauer, R., Brosch, M. & Eckhorn, R. (1995) Different rules of spatial summation from beyond the receptive field for spike rates and oscillation amplitudes in cat visual cortex. *Brain Res.*, **669**, 291–297.

Boynton, G.M., Engel, S.A., Glover, G.H. & Heeger, D.J. (1996) Linear systems analysis of functional magnetic resonance imaging in human V1. *J. Neurosci.*, **16**, 4207–4221.

Bringuier, V., Chavane, F., Glaeser, L. & Fregnac, Y. (1999) Horizontal propagation of visual activity in the synaptic integration field of area 17 neurons. *Science*, **283**, 695–699.

Brunel, N. & Wang, X.J. (2003) What determines the frequency of fast network oscillations with irregular neural discharges? I. Synaptic dynamics and excitation-inhibition balance *J. Neurophysiol.*, **90**, 415–430.

Bush, P.C. & Douglas, R.J. (1991) Synchronization of bursting action potential discharge in a model network of neocortical neurons. *Neural Comput.*, **3**, 19–30.

Buzsaki, G. (2004) Large-scale recording of neuronal ensembles. *Nat. Neurosci.*, **7**, 446–451.

Buzsaki, G. & Draguhn, A. (2004) Neuronal oscillations in cortical networks. *Science*, **304**, 1926–1929.

Carandini, M. & Heeger, D.J. (1994) Summation and division by neurons in primate visual cortex. *Science*, **264**, 1333–1336.

Cavanaugh, J.R., Bair, W. & Movshon, J.A. (2002) Nature and interaction of signals from the receptive field center and surround in macaque V1 neurons. *J. Neurophysiol.*, **88**, 2530–2546.

Daniel, P.M. & Whitteridge, D. (1961) The representation of the visual field on the cerebral cortex in monkeys. *J. Physiol.*, **159**, 203–221.
Das, A. & Gilbert, C.D. (1995) Long-range horizontal connections and their role in cortical reorganization revealed by optical recording of cat primary visual cortex. *Nature*, **375**, 780–784.
DeAngelis, G.C., Ohzawa, I. & Freeman, R.D. (1993) Spatiotemporal organization of simple-cell receptive fields in the cat's striate cortex. I. General characteristics and postnatal development. *J. Neurophysiol.*, **69**, 1091–1117.
DeAngelis, G.C., Freeman, R.D. & Ohzawa, I. (1994) Length and width tuning of neurons in the cat's primary visual cortex. *J. Neurophysiol.*, **71**, 347–374.
Delicato, L.S., Hunter, D., Sun, L. & Thiele, A. (2006). Contrast-dependent spatial integration in awake macaque V1 measured by fMRI. *Soc. Neurosci. Abstr.*, **36**, 436–438 (E446).
Dow, B.M., Snyder, A.Z., Vautin, R.G. & Bauer, R. (1981) Magnification factor and receptive field size in foveal striate cortex of the monkey. *Exp. Brain Res.*, **44**, 213–228.
Eckhorn, R., Bauer, R., Jordan, W., Brosch, M., Kruse, W., Munk, M. & Reitboeck, H.J. (1988) Coherent oscillations: a mechanism of feature linking in the visual cortex? Multiple electrode and correlation analyses in the cat *Biol. Cybern.*, **60**, 121–130.
Freiwald, W.A., Kreiter, A.K. & Singer, W. (1995) Stimulus dependent intercolumnar synchronization of single unit responses in cat area 17. *Neuroreport*, **6**, 2348–2352.
Friedman-Hill, S., Maldonado, P.E. & Gray, C.M. (2000) Dynamics of striate cortical activity in the alert macaque: I. incidence and stimulus-dependence of gamma-band neuronal oscillations. *Cereb. Cortex*, **10**, 1105–1116.
Frien, A., Eckhorn, R., Bauer, R., Woelbern, T. & Gabriel, A. (2000) Fast oscillations display sharper orientation tuning than slower components of the same recordings in striate cortex of the awake monkey. *Eur. J. Neurosci.*, **12**, 1453–1465.
Fries, P., Reynolds, J.H., Rorie, A.E. & Desimone, R. (2001) Modulation of oscillatory neuronal synchronization by selective visual attention. *Science*, **291**, 1560–1563.
Gail, A., Brinksmeyer, H.J. & Eckhorn, R. (2004) Perception-related modulations of local field potential power and coherence in primary visual cortex of awake monkey during binocular rivalry. *Cereb. Cortex*, **14**, 300–313.
Galarreta, M. & Hestrin, S. (1999) A network of fast-spiking cells in the neocortex connected by electrical synapses. *Nature*, **402**, 72–75.
Gray, C.M. & McCormick, D.A. (1996) Chattering cells: superficial pyramidal neurons contributing to the generation of synchronous oscialltions in the visual cortex. *Science*, **274**, 109–113.
Gray, C.M., König, P., Engel, A.K. & Singer, W. (1989) Oscillatory responses in cat visual cortex exhibit inter-columnar synchronization which reflects global stimulus properties. *Nature*, **338**, 334–337.
Grinvald, A., Lieke, E.E., Frostig, R.D. & Hildesheim, R. (1994) Cortical point-spread function and long-range lateral interactions revealed by real-time optical imaging of macaque monkey primary visual cortex. *J. Neurosci.*, **14**, 2545–2568.
Hammond, P. & MacKay, D.M. (1981) Modulatory influences of moving textured backgrounds on responsiveness of simple cells in feline striate cortex. *J. Physiol.*, **319**, 431–442.
Hasenstaub, A., Shu, Y., Haider, B., Kraushaar, U., Duque, A. & McCormick, D.A. (2005) Inhibitory postsynaptic potentials carry synchronized frequency information in active cortical networks. *Neuron*, **47**, 423–435.
Henrie, J.A. & Shapley, R. (2005) LFP power spectra in V1 cortex: the graded effect of stimulus contrast. *J. Neurophysiol.*, **94**, 479–490.
Herculano-Houzel, S., Munk, M.H., Neuenschwander, S. & Singer, W. (1999) Precisely synchronized oscillatory firing patterns require electroencephalographic activation. *J. Neurosci.*, **19**, 3992–4010.
Hestrin, S. & Galarreta, M. (2005) Electrical synapses define networks of neocortical GABAergic neurons. *Trends Neurosci.*, **28**, 304–309.
Hubel, D.H. & Wiesel, T.N. (1968) Receptive fields and functional architecture of monkey striate cortex. *J. Physiol.*, **195**, 215–243.
Hubel, D.H. & Wiesel, T.N. (1974) Sequence regularity and geometry of orientation columns in the monkey striate cortex. *J. Comp. Neurol.*, **158**, 267–293.
Ichida, J.M., Schwabe, L., Bressloff, P.C. & Angelucci, A. (2007) Response facilitation from the ''suppressive'' receptive field surround of macaque V1 neurons. *J. Neurophysiol.*, **98**, 2168–2181.
Johnson, R.R. & Burkhalter, A. (1994) Evidence for excitatory amino acid neurotransmitters in forward and feedback corticocortical pathways within rat visual cortex. *Eur. J. Neurosci.*, **6**, 272–286.
Jones, M.V. & Harrison, N.L. (1993) Effects of volatile anesthetics on the kinetics of inhibitory postsynaptic currents in cultured rat hippocampal neurons. *J. Neurophysiol.*, **70**, 1339–1349.
Jones, H.E., Grieve, K.L., Wang, W. & Sillito, A.M. (2001) Surround suppression in primate V1. *J. Neurophysiol.*, **86**, 2011–2028.
Kapadia, M.K., Westheimer, G. & Gilbert, C.D. (2000) Spatial distribution of contextual interactions in primary visual cortex and in visual perception. *J. Neurophysiol.*, **84**, 2048–2062.
Kayser, C. & Konig, P. (2004) Stimulus locking and feature selectivity prevail in complementary frequency ranges of V1 local field potentials. *Eur. J. Neurosci.*, **19**, 485–489.
Kayser, C., Kim, M., Ugurbil, K., Kim, D.S. & Konig, P. (2004) A comparison of hemodynamic and neural responses in cat visual cortex using complex stimuli. *Cereb. Cortex*, **14**, 881–891.
Kreiman, G., Hung, C.P., Kraskov, A., Quiroga, R.Q., Poggio, T. & DiCarlo, J.J. (2006) Object selectivity of local field potentials and spikes in the macaque inferior temporal cortex. *Neuron*, **49**, 433–445.
Kreiter, A.K. & Singer, W. (1996) Stimulus-dependent synchronization of neuronal responses in the visual cortex of the awake macaque monkey. *J. Neurosci.*, **16**, 2381–2396.
Kruse, W. & Eckhorn, R. (1996) Inhibition of sustained gamma oscillations (35-80 Hz) by fast transient responses in cat visual cortex. *Proc. Natl Acad. Sci. USA*, **93**, 6112–6117.
Levitt, J.B. & Lund, J.S. (2002) The spatial extent over which neurons in macaque striate cortex pool visual signals. *Vis. Neurosci.*, **19**, 439–452.
Li, C.Y. & Li, W. (1994) Extensive integration field beyond the classical receptive field of cat's striate cortical neurons-classification and tuning properties. *Vision Res.*, **34**, 2337–2355.
Liu, J. & Newsome, W.T. (2006) Local field potential in cortical area, MT: stimulus tuning and behavioral correlations. *J. Neurosci.*, **26**, 7779–7790.
Logothetis, N.K. (2002) The neural basis of the blood-oxygen-level-dependent functional magnetic resonance imaging signal. *Philos. Trans. R Soc. Lond. B Biol. Sci.*, **357**, 1003–1037.
Logothetis, N.K., Pauls, J., Augath, M., Trinath, T. & Oeltermann, A. (2001) Neurophysiological investigation of the basis of the fMRI signal. *Nature*, **412**, 150–157.
Maffei, L. & Fiorentini, A. (1976) The unresponsive regions of visual cortical receptive fields. *Vision Res.*, **16**, 1131–1139.
Markram, H., Toledo-Rodriguez, M., Wang, Y., Gupta, A., Silberberg, G. & Wu, C. (2004) Interneurons of the neocortical inhibitory system. *Nat. Rev. Neurosci.*, **5**, 793–807.
McGurie, B.A., Gilbert, C.D., Rivlin, P.K. & Wiesel, T.N. (1991) Targets of horizontal connections in Macaque primary visual cortex. *J. Comp. Neurol.*, **305**, 370–392.
Miller, R. (2007) Theory of the normal waking EEG: from single neurones to waveforms in the alpha, beta and gamma frequency ranges. *Int. J. Psychophysiol.*, **64**, 18–23.
Mitzdorf, U. (1987) Properties of the evoked potential generators: current source-density analysis of visually evoked potentials in the cat cortex. *Int. J. Neurosci.*, **33**, 33–59.
Mody, I., Tanelian, D.L. & MacIver, M.B. (1991) Halothane enhances tonic neuronal inhibition by elevating intracellular calcium. *Brain Res.*, **538**, 319–323.
Mukamel, R., Gelbard, H., Arieli, A., Hasson, U., Fried, I. & Malach, R. (2005) Coupling between neuronal firing, field potentials, and FMRI in human auditory cortex. *Science*, **309**, 951–954.
Nelson, J.I. & Frost, B.J. (1978) Orientation selective inhibition from beyond the classic visual receptive field. *Brain Res.*, **139**, 359–365.
Niessing, J., Ebisch, B., Schmidt, K.E., Niessing, M., Singer, W. & Galuske, R.A. (2005) Hemodynamic signals correlate tightly with synchronized gamma oscillations. *Science*, **309**, 948–951.
Nir, Y., Fisch, L., Mukamel, R., Gelbard-Sagiv, H., Arieli, A., Fried, I. & Malach, R. (2007) Coupling between neuronal firing rate, gamma LFP, and BOLD fMRI is related to interneuronal correlations. *Curr. Biol.*, **17**, 1275–1285.
de Oliveira, S.C., Thiele, A. & Hoffmann, K.P. (1997) Synchronization of neuronal activity during stimulus expectation in a direction discrimination task. *J. Neurosci.*, **17**, 9248–9260.
Palanca, B.J. & DeAngelis, G.C. (2005) Does neuronal synchrony underlie visual feature grouping? *Neuron*, **46**, 333–346.
Pesaran, B., Pezaris, J.S., Sahani, M., Mitra, P.P. & Andersen, R.A. (2002) Temporal structure in neuronal activity during working memory in macaque parietal cortex. *Nat. Neurosci.*, **5**, 805–811.
Raiguel, S., Van Hulle, M.M., Xiao, D.K., Marcar, V.L. & Orban, G.A. (1995) Shape and spatial distribution of receptive fields and antagonistic motion

surrounds in the middle temporal area (V5) of the macaque. *Eur. J. Neurosci.*, **7**, 2064–2082.
Rees, G., Friston, K. & Koch, C. (2000) A direct quantitative relationship between the functional properties of human and macaque V5. *Nat. Neurosci.*, **3**, 716–723.
Ringach, D. & Shapley, R. (2004) Reverse correlation in neurophysiology. *Cogn. Sci.*, **28**, 147–166.
Roberts, M.J., Zinke, W., Guo, K., Robertson, R., McDonald, J.S. & Thiele, A. (2005) Acetylcholine dynamically controls spatial integration in marmoset primary visual cortex. *J. Neurophysiol.*, **93**, 2062–2072.
Roberts, M., Delicato, L.S., Herrero, J., Gieselmann, M.A. & Thiele, A. (2007) Attention alters spatial integration in macaque V1 in an eccentricity-dependent manner. *Nat. Neurosci.*, **10**, 1483–1491.
Roelfsema, P.R., Lamme, V.A. & Spekreijse, H. (2004) Synchrony and covariation of firing rates in the primary visual cortex during contour grouping. *Nat. Neurosci.*, **7**, 982–991.
Sceniak, M.P., Ringach, D.L., Hawken, M.J. & Shapley, R. (1999) Contrast's effect on spatial summation by macaque V1 neurons. *Nat. Neurosci.*, **2**, 733–739.
Sceniak, M.P., Hawken, M.J. & Shapley, R. (2001) Visual spatial characterization of macaque V1 neurons. *J. Neurophysiol.*, **85**, 1873–1887.
Scherberger, H., Jarvis, M.R. & Andersen, R.A. (2005) Cortical local field potential encodes movement intentions in the posterior parietal cortex. *Neuron*, **46**, 347–354.
Shao, Z. & Burkhalter, A. (1996) Different balance of excitation and inhibition in forward and feedback circuits of rat visual cortex. *J. Neurosci.*, **16**, 7353–7365.
Shao, Z. & Burkhalter, A. (1999) Role of GABAB receptor-mediated inhibition in reciprocal interareal pathways of rat visual cortex. *J. Neurophysiol.*, **81**, 1014–1024.
Singer, W. (1999) Neuronal synchrony: a versatile code for the definition of relations. *Neuron*, **24**, 49–65.
Swindale, N.V. (1991) Coverage and the design of striate cortex. *Biol. Cybern.*, **65**, 415–424.
Tamas, G., Buhl, E.H., Lorincz, A. & Somogyi, P. (2000) Proximally targeted GABAergic synapses and gap junctions synchronize cortical interneurons. *Nat. Neurosci.*, **3**, 366–371.
Thiele, A. & Stoner, G. (2003) Neuronal synchrony does not correlate with motion coherence in cortical area MT. *Nature*, **421**, 366–370.
Thiele, A., Delicato, L.S., Roberts, M.J. & Gieselmann, M.A. (2006) A novel electrode-pipette design for simultaneous recording of extracellular spikes and iontophoretic drug application in awake behaving monkeys. *J. Neurosci. Methods*, **158**, 207–211.
Tiesinga, P.H. & Sejnowski, T.J. (2004) Rapid temporal modulation of synchrony by competition in cortical interneuron networks. *Neural Comput.*, **16**, 251–275.
Tootell, R.B., Switkes, E., Silverman, M.S. & Hamilton, S.L. (1988) Functional anatomy of macaque striate cortex. II. Retinotopic organization. *J. Neurosci.*, **8**, 1531–1568.
Traub, R.D., Whittington, M.A., Colling, S.B., Buzsaki, G. & Jefferys, J.G. (1996a). Analysis of gamma rhythms in the rat hippocampus in vitro and in vivo. *J. Physiol.* **493** (Pt. 2), 471–484.
Traub, R.D., Whittington, M.A., Stanford, I.M. & Jefferys, J.G.R. (1996b) A mechanism for generation of long-range synchronous fast oscillations in the cortex. *Nature*, **383**, 621–624.
Wang, X.J. & Buzsaki, G. (1996) Gamma oscillation by synaptic inhibition in a hippocampal interneuronal network model. *J. Neurosci.*, **16**, 6402–6413.
Whittington, M.A. & Traub, R.D. (2003) Interneuron diversity series: inhibitory interneurons and network oscillations in vitro. *Trends Neurosci.*, **26**, 676–682.
Wilke, M., Logothetis, N.K. & Leopold, D.A. (2006) Local field potential reflects perceptual suppression in monkey visual cortex. *Proc. Natl Acad. Sci. USA*, **103**, 17507–17512.
Williams, A.L., Singh, K.D. & Smith, A.T. (2003) Surround modulation measured with functional MRI in the human visual cortex. *J. Neurophysiol.*, **89**, 525–533.
Wilson, J.R. & Sherman, S.M. (1976) Receptive-field characteristics of neurons in cat striate cortex: changes with visual field eccentricity. *J. Neurophysiol.*, **39**, 512–533.
Woelbern, T., Frien, A., Eckhorn, R., Bauer, R. & Kehr, H. (1994) Distribution of oscillation frequencies depend on stimulus size and velocity in monkey visual cortex. In Elsner, N. & Breer, H. (Eds), *Sensory Transduction*. Thieme, New York, p. 337.
Womelsdorf, T., Fries, P., Mitra, P.P. & Desimone, R. (2006) Gamma-band synchronization in visual cortex predicts speed of change detection. *Nature*, **439**, 733–736.
Zenger-Landolt, B. & Heeger, D.J. (2003) Response suppression in V1 agrees with psychophysics of surround masking. *J. Neurosci.*, **23**, 6884–6893.